Effect of a high-voltage mesh electrode on the volume and surface characteristics of pulsed dielectric barrier discharges

Document license:
TAVERNE

DOI:
[10.1063/5.0032342](#)

Document status and date:
Published: 01/01/2020

Document Version:
Publisher's PDF, also known as Version of Record (includes final page, issue and volume numbers)

Please check the document version of this publication:

• A submitted manuscript is the version of the article upon submission and before peer-review. There can be important differences between the submitted version and the official published version of record. People interested in the research are advised to contact the author for the final version of the publication, or visit the DOI to the publisher's website.
• The final author version and the galley proof are versions of the publication after peer review.
• The final published version features the final layout of the paper including the volume, issue and page numbers.

[Link to publication](#)

Effect of a high-voltage mesh electrode on the volume and surface characteristics of pulsed dielectric barrier discharges

M. Kettlitz, O. van Rooij, H. Höft, R. Brandenburg, and A. Sobota

COLLECTIONS

View Online   Export Citation   CrossMark

ARTICLES YOU MAY BE INTERESTED IN

Effect of a high-voltage mesh electrode on the volume and surface characteristics of pulsed dielectric barrier discharges Ⓕ

M. Kettlitz,[1,a)] ⓘD O. van Rooij,[2] H. Höft,[1] ⓘD R. Brandenburg,[1] ⓘD and A. Sobota[2,b)] ⓘD

AFFILIATIONS

[1]Leibniz Institute for Plasma Science and Technology (INP), Felix-Hausdorff-Str. 2, 17489 Greifswald, Germany
[2]Department of Applied Physics, Eindhoven University of Technology, EPG, Postbus, 513, 5600MB Eindhoven, The Netherlands

Note: This paper is part of the Special Topic on Fundamentals and Applications of Atmospheric Pressure Plasmas.
[a)]**Author to whom correspondence should be addressed:** kettlitz@inp-greifswald.de
[b)]a.sobota@tue.nl

ABSTRACT

Electrical breakdown in a pulsed asymmetric dielectric barrier discharge between a glass-covered mesh electrode and a grounded metal electrode in the air at atmospheric pressure is investigated. Volume discharge forms between the metal tip and the dielectric surface and spreads over the dielectric surface. Breakdown and discharge behaviors depend on the polarity of the charged electrode covered with glass compared to the metal rod electrode. In the case of the dielectric cathode (covered mesh), volume discharge features a stronger and longer-lasting emission. Volume discharge is weaker with outstretched surface discharge developing on the opposite glass electrode sustained by the embedded mesh when the metal rod functions as a cathode. The development and spatial distribution of the surface discharge depend on the relative polarity of the dielectrics caused by the charge deposition of the preceding discharge and is independent of the polarity of the applied high voltage. The discharge emission is brighter for the metal cathode and dielectric anode than for the metal anode, with a branching discharge developing and spreading in a star-like structure along the embedded grid, while a ring-like structure was observed for the metal anode and dielectric cathode. The duty cycle influences the discharge development and properties through the effects of the gas phase and surface pre-ionization.

I. INTRODUCTION

Due to their operation at atmospheric pressure and their scalability, dielectric barrier discharges (DBDs) have many different applications. Plate-to-plate DBD arrangements are useful for large scale applications such as activation and treatment of sheets. Homogeneous plasma formation, especially on the surface, is of major importance for a smooth operation of the DBD.[1,2] Not only diffuse DBDs are interesting approaches for this issue but also filamented DBDs with "diffuse" foot points spread over the surface. Self-organization of filamented DBDs has been investigated in this context, especially the formation and the breakdown mechanism of the barrier discharge and the memory effects.[3]

Plasma medicine is an emerging field, and the first DBD-based devices for the wound and skin treatment have already

been introduced in the market.[4–11] However, the surface of the human body is anything but homogeneous or regular, which has motivated the design of flexible DBDs, e.g., a surface DBD incorporating thin ($50\,\mu$m) polymer dielectric barriers.[12] Another problem is the filamentary and, thus, erratic structure of the DBD in most molecular gases, including the air. An attempt to improve the surface uniformity of filamentary DBDs is the use of thin mesh electrodes covered by a dielectric.[13–18] The thin dielectric layer, on the one hand, prevents the discharge from the transition to a spark and, on the other hand, does not blur the electric field structure of the embedded mesh that much. In combination with a thin dielectric barrier, distinct but uniformly distributed spots with a maximum electric field strength are present in the discharge gap near the surface. The use of metal and dielectric electrodes in one
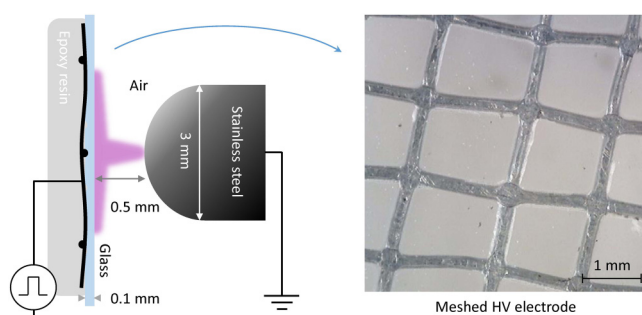
FIG. 1. The plasma source consists of a fine-meshed charged electrode covered by a 0.1 mm thick glass plate serving as a dielectric layer and a grounded rod. The mesh is slightly irregular, with an average spacing between wires of about 1 mm.

arrangement leads to asymmetric discharges with higher discharge intensity and streamer velocities.[19]

However, fundamental questions on the role of the thin barrier, the influence of the surface and pre-ionization,[19–22] the morphology of single filaments, and the properties of microdischarges including basic quantities as number densities, electron and gas temperatures, and the electric filed strength for special configurations are current research objects.[23–31]

The aim of this study is to investigate the discharge behavior in the volume and on the surface of an asymmetric DBD with a thin dielectric layer covering a fine mesh electrode and analyze the coaction of volume and surface discharges. We concentrate on the influences of the electrode polarity on the discharge and on the plasma distribution on the surface, the embedded grid on the surface discharge, and the pre-ionization on the discharge morphology by variation of the duty cycle of pulsed DBDs.

II. EXPERIMENTAL SETUP

The asymmetric dielectric barrier discharge arrangement for this study is shown in Fig. 1. A fine rectangular mesh of 0.1 mm thickness wires spaced about 1 mm apart served as the charged electrode. The mesh was embedded in an epoxy resin and covered by a sheet of 0.1 mm thick glass. The glass cover served as the dielectric barrier and the epoxy resin prevented the mesh from coming in contact with the air and breaking down at unwanted places. The mesh was placed horizontally with the glass layer on top of it. A metal rod with a spherical tip and a diameter of 3 mm served as the ground electrode. To obtain spatially stable discharges, it was placed 0.5 mm away from the glass barrier and vertically aligned above a junction of the grid.

The discharge was driven by a high-voltage (HV) pulser producing pulses of 8 kV amplitude at a repetition frequency (f_{rep}) of 4.88 kHz. The steepness of the rising and falling slopes of the high-voltage pulses was about 200 V/ns, specified by the pulse generator (DEI PVX-4110) powered by a DC HV source (FuG HCN 1400-12500), triggered by a pulse delay generator (SRS DG535) (see Fig. 2), similar to as described in Ref. 32. Even though measurements were performed at a range of duty cycles between 5% and 95%, for the sake of clarity, this paper presents only the 10%, 50%, and 90% duty cycles, i.e., pulses of $20\,\mu s$, $102.5\,\mu s$, and $185\,\mu s$ duration (see Fig. 4). The discharges were generated in the open air at atmospheric pressure with humidity below 40%. The downward airflow of about 0.4 m/s was generated by a fan (Delta electronics, FFB0412VHN) close to the discharge.

Electrical measurements were performed with fast voltage (Tektronix P6015A) and current probes (Pearson 2877) at the HV and grounded side and recorded with a digital phosphor oscilloscope (Tektronix TDS 7254). Images of the DBDs were recorded in the visible spectral range with a fast ICCD camera (Andor iStar, $\Delta t \geq 2\,ns$, $\Delta x < 10\,\mu m$) with a commercial objective (Canon Compact-Macro 50 mm f/2.5), as shown in Fig. 2. The camera was set either to 90° to observe the side-on emission of volume discharges or to 60° to observe both volume and surface discharges (Fig. 2). Furthermore, the spatiotemporal development of the volume discharge was recorded side-on with a streak camera (Hamamatsu C5680). The streak camera measurements were performed spectrally integrated in the UV and VIS spectral range. A long-distance microscope (Questar QM100) was used to obtain a high spatial resolution of the volume discharge.
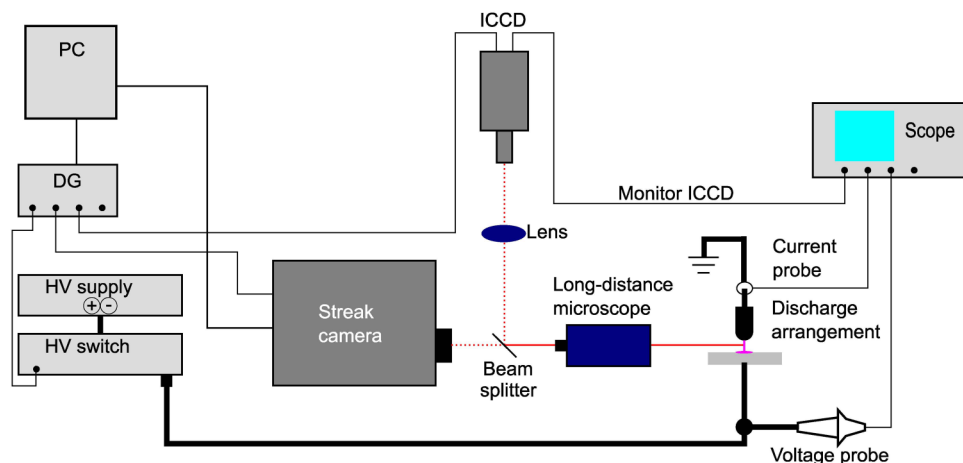

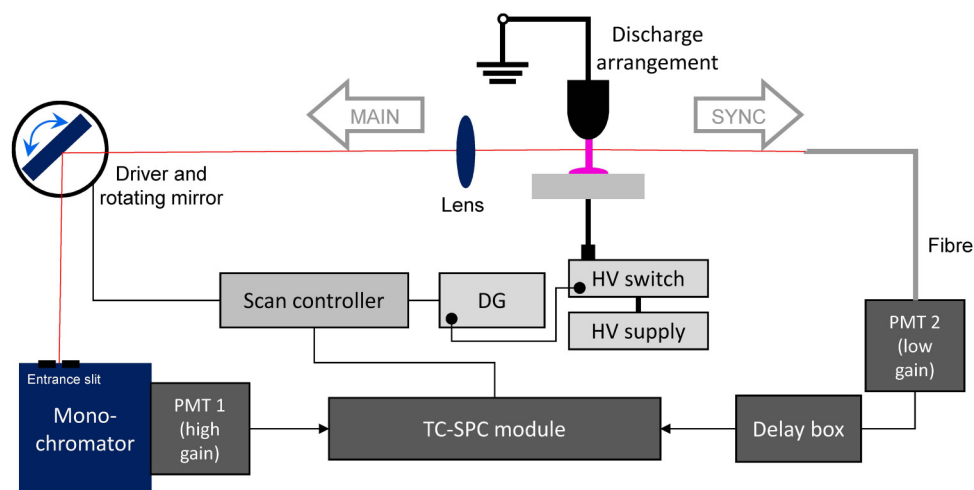**FIG. 2.** Experimental setup with electrical and optical equipments.

FIG. 3. Setup for cross-correlation spectroscopy (CCS).

The spatiotemporal emission of the second positive system (SPS) of N_2 and of the first negative system (FNS) of N_2^+ was recorded by cross-correlation spectroscopy (CCS) [or time-correlated single photon counting (TC-SPC)],[33] in a similar diagnostic setup as described in Refs. 19 and 34. The CCS method allows the real-time measurement of the discharge event to be substituted by a statistically averaged determination of the cross-correlation function between two optical signals, the main signal and the synchronization signal, both originating from the same source. The main signal contains the data to be recorded, while the synchronization signal came from the light in the visible spectral range observed from the discharge. The time intervals between the detection of the signals are measured, resulting in a time histogram of counted photons of the discharge. Details of the CCS technique are described in Ref. 35. The advantages of this method include its higher sensitivity compared to streak camera measurements and usefulness for discharges that have a statistical jitter. However, it requires data to be recorded for a considerable amount of time (stable conditions over hours). The CCS setup is pictured in Fig. 3.

It consisted of a time-correlated single photon counting module (Becker&Hickl SPS-150) and two sensitive photomultiplier tubes (PMTs) (Hamamatsu PMC-100-4). The main signal was imaged to the entrance slit of a 0.25 m-monochromator (Princeton Instruments SP-2300) with a grating of 2400 g/mm to record spectrally resolved emission from the discharge with PMT1. A flipping mirror scanned the discharge along the axis. The synchronization signal was collected by a light fiber, recorded with PMT2, and transmitted to the TC-SPC module via a delay box. The scanning mirror driver and the memory segments of the TC-SPC module were synchronized by a scan controller. The CCS measurements were performed for two transitions in nitrogen: the 0–3 transition of the second positive system of N_2,

$$N_2\left(C^3\Pi_u\right)_{v'=0} \longrightarrow N_2\left(B^3\Pi_g\right)_{v''=0} + h\nu_{0-3}^{\text{SPS}}, \tag{1}$$
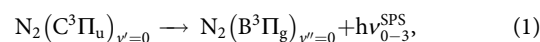
at $\left(\lambda_{0-3}^{\text{SPS}} = 405\,\text{nm}\right)$ with an excitation energy of $\Delta E = 11.03\,\text{eV}$[36] and the 0–0 transition of the first negative system of N_2^+,
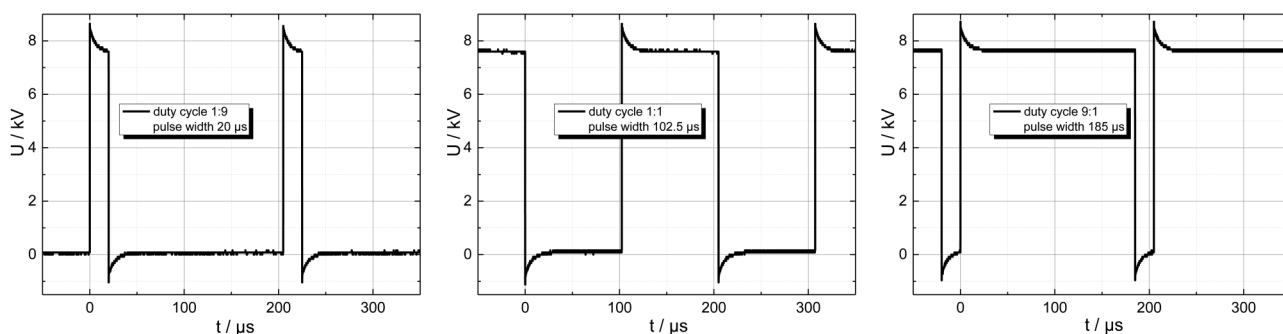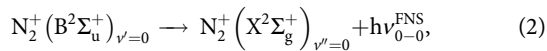

FIG. 4. Applied voltage pulses for duty cycles of 1:9, 1:1, and 9:1; (10%, 50%, and 90%, i.e., pulse durations of 20 μs, 102.5 μs, and 185 μs).

$$N_2^+ \left(B^2\Sigma_u^+\right)_{v'=0} \longrightarrow N_2^+ \left(X^2\Sigma_g^+\right)_{v''=0} + h\nu_{0-0}^{FNS}, \qquad (2)$$

at $\left(\lambda_{0-0}^{FNS} = 391.44 \, \text{nm}\right)$ with an excitation energy of $\Delta E = 18.75 \, \text{eV}$.[36]

The SPS contributed to the major part of the emission, while the FNS was correlated to the region of high electric field strength (i.e., high energetic electrons) due to its high excitation energy.

III. RESULTS AND DISCUSSION

A. Electrical measurements

Figure 4 shows the applied positive high-voltage pulses for three different duty cycles (pulse widths). During the rising slope and the falling slope of the applied voltage pulse, only one discharge occurred for each slope. Hence, the delay time between the two discharges ($20 \, \mu s$–$185 \, \mu s$) determined the precondition in terms of reactive species, residual charges in the gap, and on the dielectric surface for the following discharge event. This way, the discharge could be controlled by the pulse width.[32,37,38]

Figure 5 shows the current–voltage characteristics during the rising slope (RS) and the falling slope (FS) of $+8 \, \text{kV}$ for duty cycles of 1:9 and 9:1, measured at the grounded side. Displayed are about 10 000 subsequent discharges saved in one oscilloscope curve (fast acquisition mode of Tektronix TDS 7254), to show the statistics of discharges in both slopes and duty cycles. During the rising slope of the unipolar positive HV pulse, the dielectric surface above the mesh acted as the anode (D^+) and the metal rod electrode as the cathode (M^-). When the glass surface above the mesh was
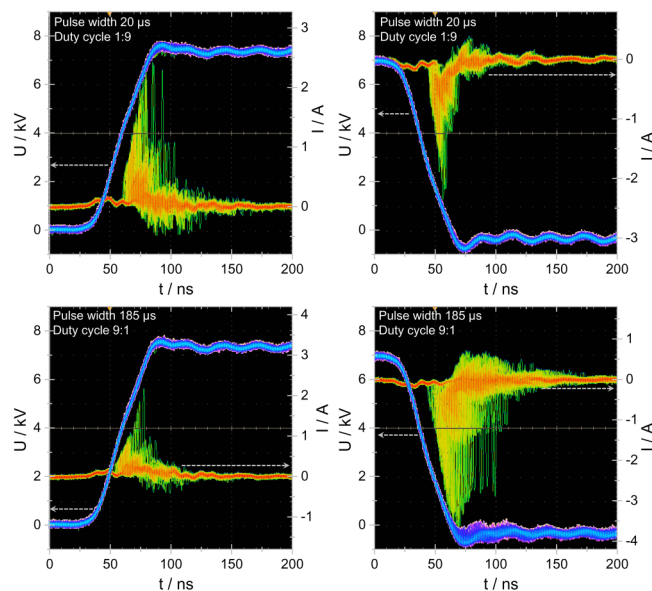

FIG. 5. Screen shot (fast acquisition mode) of the current–voltage characteristics of the rising and falling slopes for duty cycles of 1:9 and 9:1; measured at grounded side and over approximately 10 000 discharges; the relative frequency is color-coded.

charged, the surface charge caused an electric field that countered the applied electric field imposed by the electrode system, extinguishing the discharge. During the falling slope, the applied voltage dropped to 0; hence, the residual charges on the glass generated an electric field sufficient for a breakdown.[39] In this case, the covered mesh electrode functioned as a cathode (D^-) (see the polarity of the current in Fig. 5).

The total current consisted of the discharge plus the displacement current. The displacement current at the HV side was higher due to the higher capacitance of the HV cord and of the grid including the resin of the charged electrode compared to the grounded rod electrode. The current peak was about 1 A for the rising slope for duty cycles of 1:9 and 1:1. The current dropped for a duty cycle of 9:1, i.e., for a decrease in the delay to the preceding pulse of $20 \, \mu s$ due to the higher pre-ionization of the gap as explained in Ref. 37. The residual ionization effect is similar to that in classical DBDs.

When applying negative voltage pulses to the meshed electrode, the pulse amplitude was $-8 \, \text{kV}$, while other settings remained the same. The current–voltage characteristics of the drop of the voltage from 0 to $-8 \, \text{kV}$ in the negative pulses and the drop of the voltage from $+8 \, \text{kV}$ to 0 in the positive pulses were very similar. Likewise, the increase of voltage in one polarity closely resembled the decrease of voltage in the other polarity. These effects can be explained by the conditions being actually set by the charging of the surface,[39] rather than the applied voltage. The electrons that were left on the dielectric by the previous discharge served as a rich source of pre-ionization. Consequently, the polarity applied was irrelevant, as long as the electric field was high enough to ensure discharge inception in the gap. Due to lower mobility, and thus slower recombination, the availability of electrons was much higher on the dielectric than in the gas volume. Therefore, the abundance of electrons on the glass surface to form electron avalanches made the difference between the positive and the negative streamers negligible.

An estimate of the dissipated energy in the discharge gives $(40 \pm 10) \, \mu J$ per pulse. From the discharge current integrals and the applied voltage of 8 kV, the amount of charge is estimated at $(6 \pm 2) \, \text{nC}$.

B. Behavior of the volume discharge

The breakdown and discharge morphology depends on the polarity of the charged electrode (mesh) compared to the metal rod electrode. Figure 6 presents side-on ICCD images of the volume discharge of $+8 \, \text{kV}$ at rising and falling slopes for all duty cycles at a gap of 0.5 mm recorded in the ultraviolet and visible spectral range. Voltage waveforms for all duty cycles are included for clarity. Displayed are single shots and accumulated images at both the rising and the falling slope, with an exposure time of $5 \, \mu s$, tagged by gray bars in the voltage waveforms. The charged mesh is located on the left-hand side and the grounded metal rod on the right-hand side. The electrode polarity is indicated by $M^{+/-}$ (metal rod, grounded) and $D^{-/+}$ (dielectric, charged mesh). Note the reflections of the volume discharge left on the glass surface above the mesh.
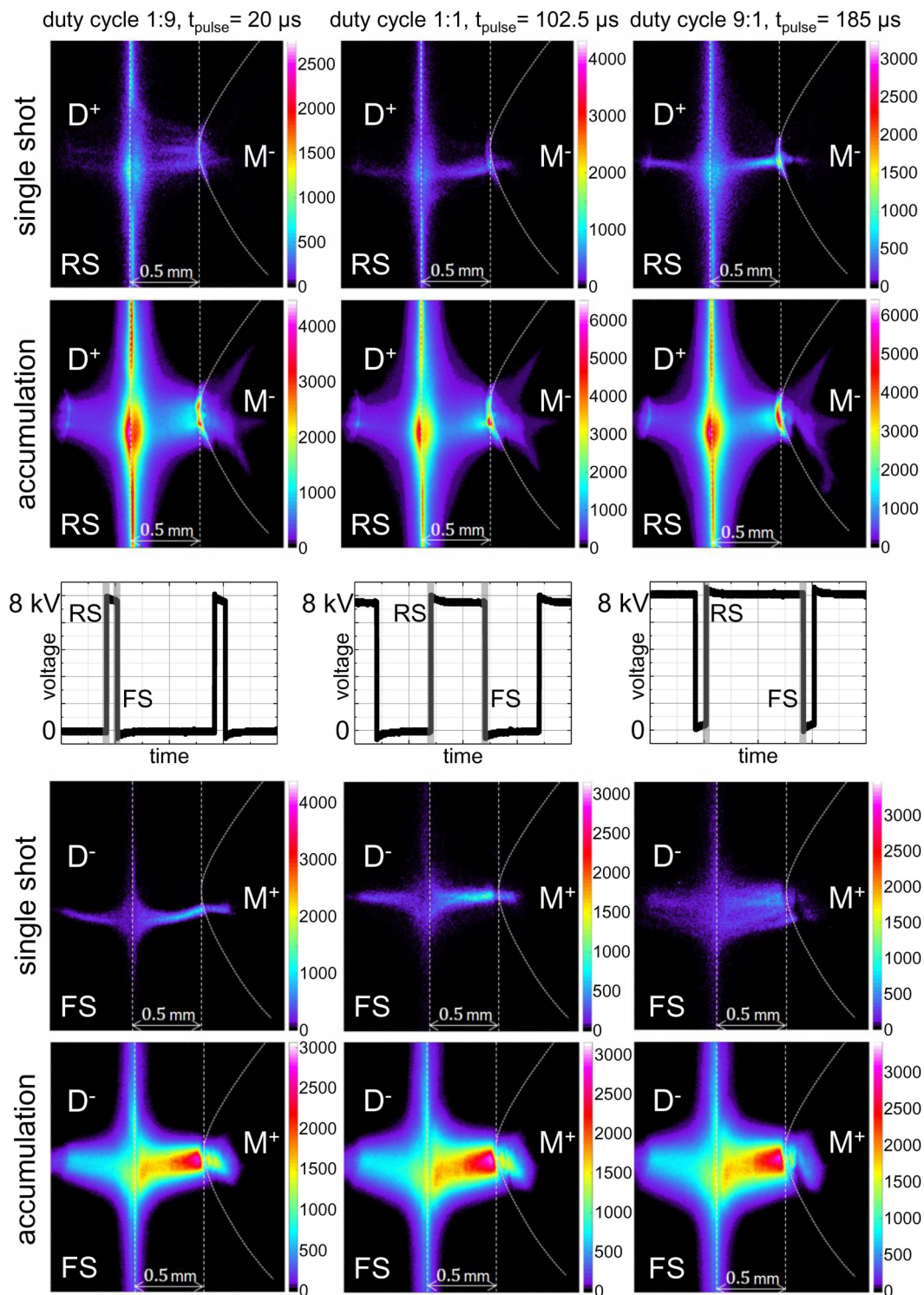
FIG. 6. Side-on ICCD images of the volume discharge (single shots and accumulations) at rising (RS) and falling (FS) slopes for all duty cycles; electrode polarity indicated by $M^{+/-}$ and $D^{-/+}$; electrode and mesh positions are marked by dotted lines; gap 0.5 mm; gate width 5 μs.

The rod was adjusted opposite to a junction of the grid and the discharge always formed between the metal rod and the dielectric surface on a junction of the mesh under the glass. A channel was generated in the volume, which subsequently spread over the dielectric surface onto a much larger area. The surface discharge always expanded from the grid junction directly under the grounded electrode and followed the geometry of the mesh, for both polarities (to be further discussed in Sec. III C). A pronounced structure in the volume could be recognized during the falling slope, when the metal rod was the anode (M^+D^-) with the highest emission intensity in front of the anode. The emission intensity at the surface of the electrodes was weaker for the FS than the RS. In the case of the rising slope, the discharge emission was less intense in the volume, while the highest intensity was obtained at the electrodes. The single shots show one or multiple constricted discharge channels in the gap (see Fig. 6 RS 1:9; FS 9:1). The discharge diameter in the volume was about $100\,\mu m$.

The pre-ionization had a visible effect on the discharge behavior. The pre-ionization increased with a shorter delay (20–$185\,\mu s$) to the preceding discharge,[37–39] causing a little decrease in the discharge diameter in the center of the discharge (see single shots in Fig. 6). For the rising slope, this decrease occurred with an increase in the duty cycle, while for the falling slope with a decrease in the duty cycle. For comparison, during a relatively long pre-breakdown phase for sinusoidal driven DBDs, Hoder *et al.*[37] found that residual surface charges on the dielectrics caused local field enhancement and promoted electron emission, leading to higher pre-ionization. Although the experiments presented here did not involve such a long period due to the steep gradient of the applied HV pulse,[38,39] the influence of residual surface charges was still visible.

To obtain the temporal behavior of the discharge development in the volume, streak camera recordings were made along the central gap axis with a radial extension of about $20\,\mu m$ of the discharge center, as described in, e.g., Ref. 32. The subsequent development of the surface discharge visible in Fig. 6 could not be detected by the streak camera because of the limited field of view of the center region of the discharge and at the surface foot point.

Figures 7 and 8 show streak images for the rising and falling slopes of a positive 9:1 pulse. Displayed are single shot and accumulated recordings. Figure 7 shows that the discharge in the rising slope was initiated in the volume and streamer development toward both electrodes within about 0.5 ns could be observed. A long-lasting surface discharge could be recognized on the glass surface. During the falling slope (Fig. 8), the discharge started in the volume closer to the rod and a cathode directed streamer to the mesh could be noticed. No pronounced long-lasting discharge on the glass surface (D^-) was detected. This effect was due to the grounded metal electrode, where no charge collection took place, because of the instant withdrawal of electrons by the circuit. This behavior is different from symmetrical DBDs, which display symmetrical pictures for 1:9 (RS) and 9:1 (FS).[32] A similar behavior was observed in Ref. 19 for asymmetrical DBDs, where the highest velocity of the ionization front was found for the metallic cathode (M^-D^+). It is assumed in Ref. 19 that for a dielectric cathode, the positive head of the ionization front is decelerated by charges on the glass surface. However, due to pulsed high-voltage,[39] streamer velocities in Ref. 19 were not as high as in the current experiment
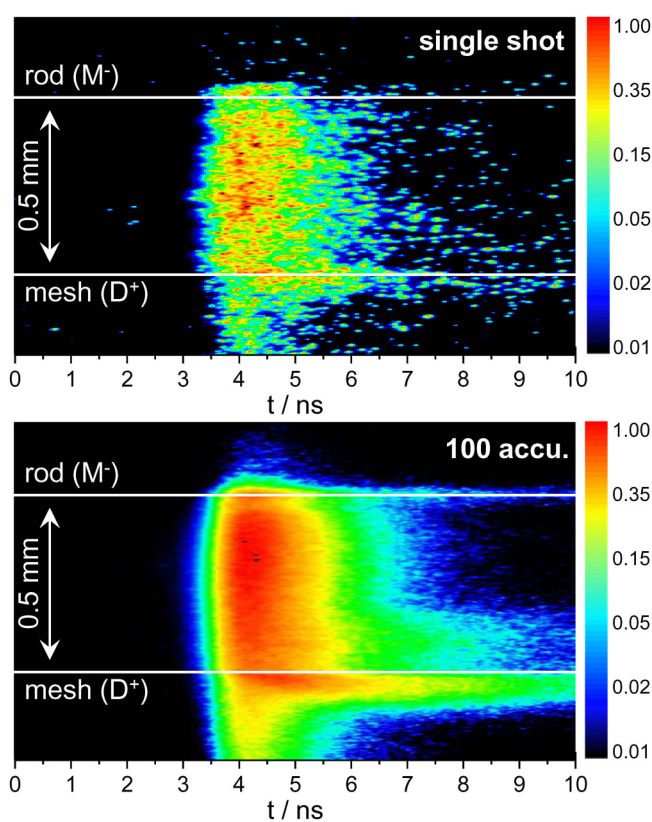

FIG. 7. Streak images for positive voltage at a duty cycle of 9:1 during the rising slope (M^-D^+); single shot record (on top) and accumulated ones (below).

with $2 \times 10^6\,ms^{-1}$ for the rising slope and $4 \times 10^6\,ms^{-1}$ for the falling slope (duty cycle 9:1).

To obtain a better insight into the breakdown behavior of the volume discharge, CCS measurements were conducted for the SPS of N_2 and the FNS of N_2^+. The SPS contributes to the major part of the emission and can be directly compared to the streak camera measurements. However, the FNS is dominantly excited by direct electron collisions with a threshold energy of about 19 eV in such microdischarges. Only electrons in high electric field regions can gain such energies. Furthermore, the effective live time of the $N_2^+(B)$ state is in the range of 0.1 ns due to collisional quenching. Thus, the FNS emission is correlated to the propagation of the electric field strength (Ref. 19).

The CCS measurements were conducted for the same gap of 0.5 mm but for a lower voltage of $+5.6\,kV$ and a duty cycle of 9:1 ($185\,\mu s$). It was not possible to conduct CCS measurements for the same voltage used for all other measurements (8 kV) due to interfering signals from the discharge arising from the high displacement current during the slopes. The interference could be avoided when operating at lower voltages, but this led to an inception delay and a shift of the discharge current to the plateaus of the pulse away from the voltage slopes with a high disturbing displacement
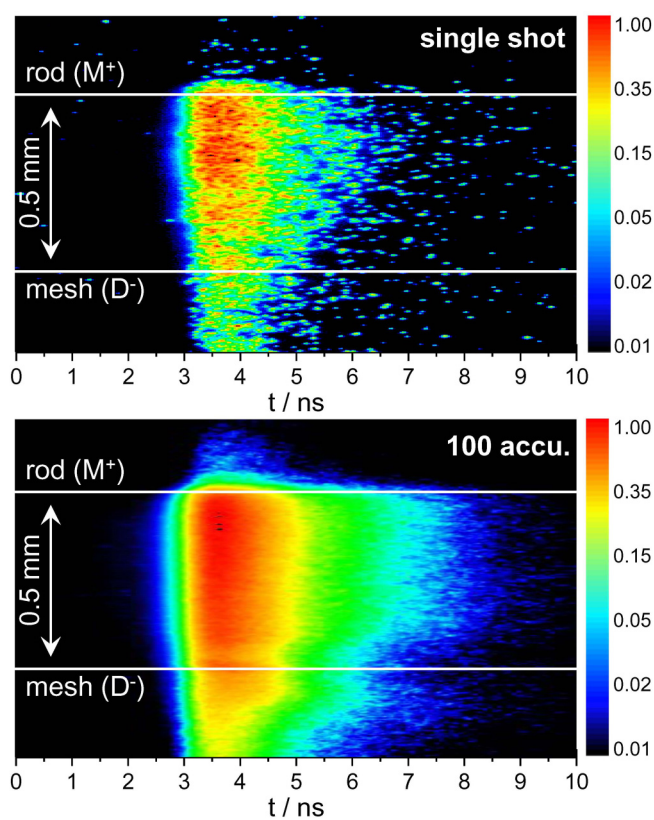
FIG. 8. Streak images for positive voltage at a duty cycle of 9:1 during the falling slope (M^+D^-); single shot record (on top) and accumulated ones (below).

current. In addition, a discharge did not occur at 5.6 kV at every voltage cycle, which led to higher currents at the next discharge. Nevertheless, the voltage rise time, as well as the basic roles of the grounded electrode, the charged mesh and the glass dielectric, remained the same for both higher and lower voltage settings. Therefore, we will use the additional information from the emission from the FNS and the SPS of nitrogen to substantiate the discussion on the role of the electric field in this discharge.

Figures 9 and 10 show CCS images for +5.6 kV at a duty cycle of 9:1 during the rising slope and the falling slope. Displayed are the SPS and the FNS. The SPS data confirm the results for the volume discharges obtained with the streak camera recordings with +8 kV for both slopes regarding volume discharge behavior and duration and surface discharge development. Here again, the surface discharge was observed to last longer during the rising slope than during the falling slope. The FNS, representing the high electric field component of the discharge, behaved differently. The duration of the FNS emission was much shorter than that of the SPS emission. High signal intensity, comparable to high electric field strength, was observed at the cathode in both cases, regardless whether this was the metallic rod or the dielectric surface but, lasted longer in the case of the dielectric cathode (D^-). It can be concluded that during the rising slope, the highest E-field strength and the highest energy electrons occurred at the grounded electrode, while the discharge on the surface was driven by lower-energy electrons in a lower E-field. During the falling slope, the highest E-field region was on the mesh, resulting in a more widespread surface discharge. The duration of the discharge emission was calculated from streak camera recordings. It was different at rising and falling slopes, and also depended on the duty cycle, as summarized in Fig. 11. The discharge in the volume during the falling slope (M^+D^-) lasted about 2.5 ns (FWHM), while the filament on the rising slope (M^-D^+) emitted light in the visible
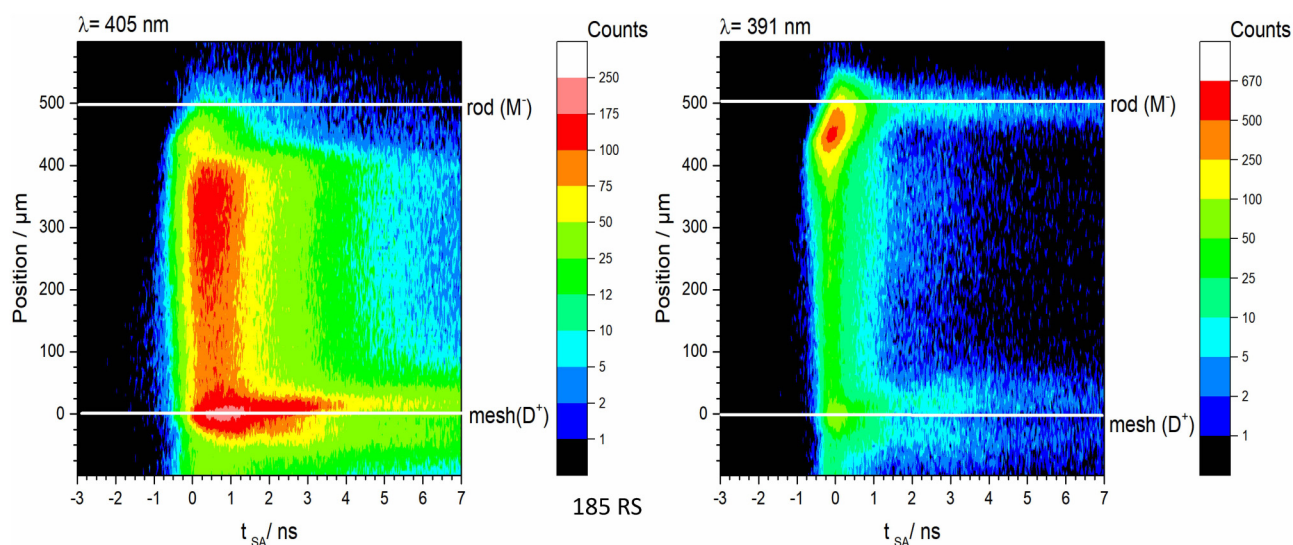

FIG. 9. CCS images for +5.6 kV at a duty cycle 9:1 during the rising slope (M^-D^+); left: SPS, right: FNS; counted photons in the logarithmic scale.
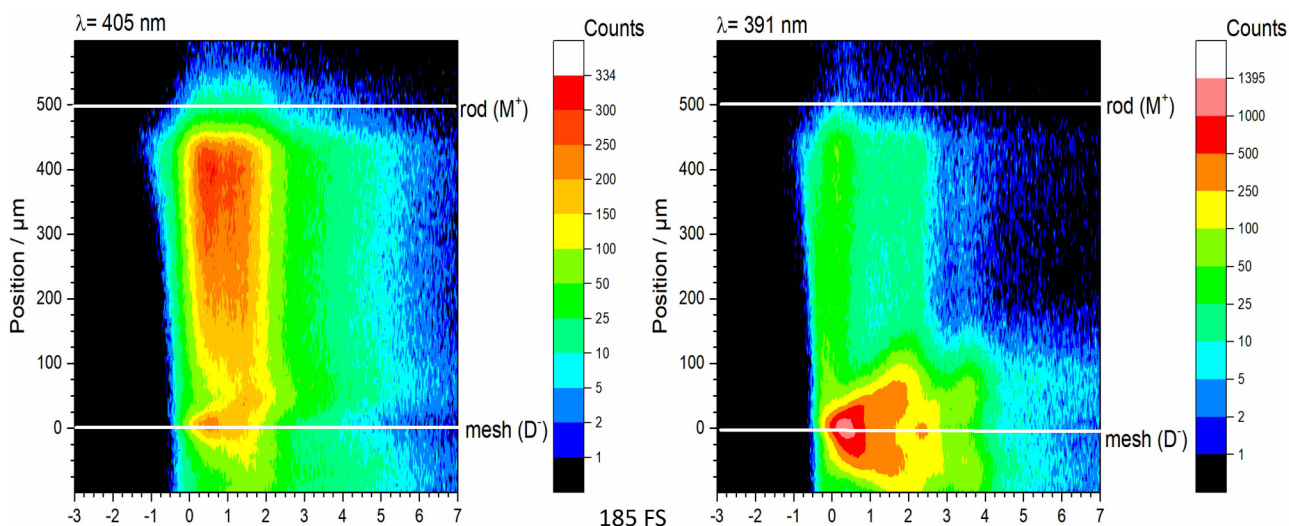
FIG. 10. CCS images for +5.6 kV at a duty cycle 9:1 during the falling slope (M^+D^-); left: SPS, right: FNS; counted photons in the logarithmic scale.

spectral range for less than 1.6 ns for a duty cycle of 1:9. The emission duration for a duty cycle of 9:1 was equal for both slopes and lasted about 1.8 ns (Figs. 7, 8, and 11). Similar behavior was observed by Hoder et al.[19] They found the decay of the discharge of the configuration with the metallic anode (M^+D^-) to be the slowest one. Calculations of Braun et al.[40] and Gibalov et al.[41] for similar arrangements with a larger gap confirm the longer emission for the metallic anode.

C. Behavior of the surface discharge

Figure 12 presents ICCD images of volume and surface discharges on the dielectrics for rising and falling slopes of +8 kV at a duty cycle of 1:9 obtained in the visible spectral range using an
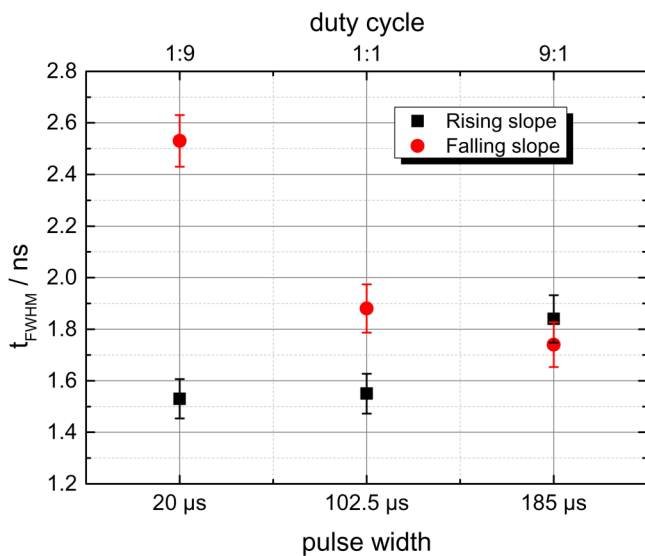
FIG. 11. Duration of spectrally integrated discharge emission of rising and falling slopes of +8 kV in dependence of the duty cycle, obtained from streak images.
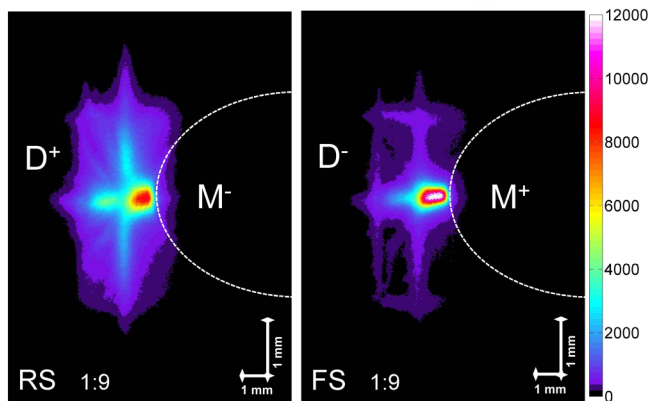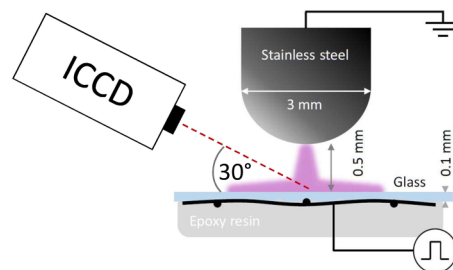
FIG. 12. Morphology of the surface discharges on the dielectrics for a duty cycle of 1:9 using an oblique projection (sketch on top; gate width of $5\,\mu s$).

FIG. 13. Temporal development of the surface discharge for + 8 kV and a duty cycle of 9:1 during the rising slope (M^-D^+) using a 10 ns ICCD gate window (accumulation on the chip); starting gate position t_0 indicated in the corresponding voltage–current waveform on top; from $t_0 + 130$ ns, the ICCD gain was increased to visualize the weak emission up to approximately $5\,\mu$s.

FIG. 14. Temporal development of the surface discharge for +8 kV and a duty cycle of 1:9 during the falling slope (M^+D^-) using a 10 ns ICCD gate window (accumulation on the chip); starting gate position t_0 indicated in the corresponding voltage–current waveform below; from $t_0 + 40$ ns, the ICCD gain was increased to visualize the weak emission up to approximately 5 μs.

oblique projection shown in the schematic diagram on top. The glass covered mesh is displayed on the left- and the metal rod on the right-hand side. The surface discharges were clearly brighter during the rising slope, when the dielectric surface was the anode, than during the falling slope, when the rod was the anode. In both cases, the outstretched surface discharge on the glass layer followed mostly the geometry of the embedded mesh. Van der Schans et al.[18] also observed that the surface discharge in their experiments followed the pattern of the mesh. In contrast to our findings, Ye et al.[17] did not notice a real spreading of surface discharges in their experiment with sinusoidal HV but only a punctual attachment (spots) at grid nodes. Surface discharges were repeatable but had diverse morphology for both polarities and developed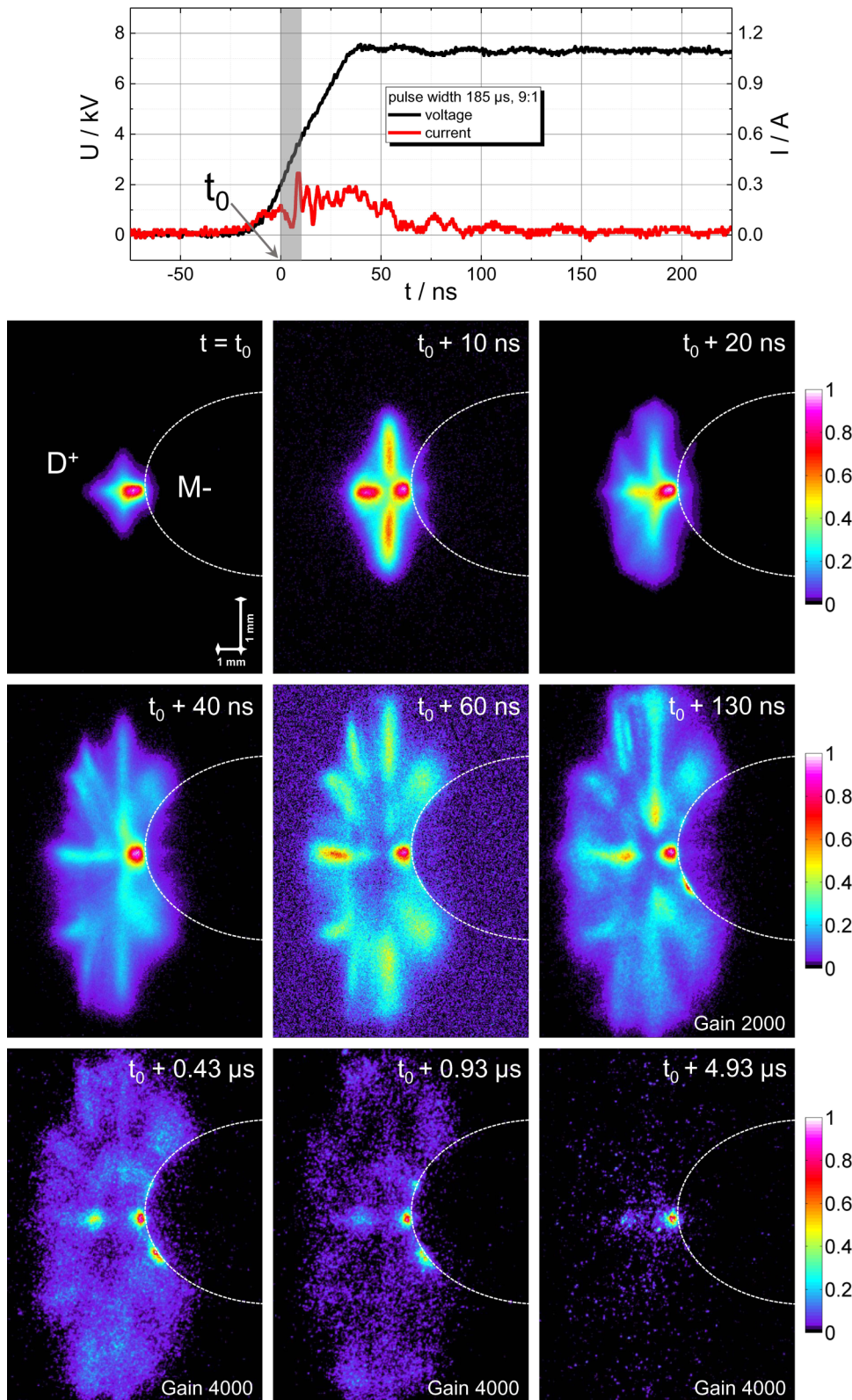 also differently along the underlying grid. Figure 13 displays the temporal development of the surface discharge for +8 kV and a duty cycle of 9:1 during the rising slope (M^-D^+) using a 10 ns ICCD gate window for each image of 1000 accumulated discharges obtained in the visible spectral range. The starting gate position t_0 is indicated in the corresponding voltage–current waveform on top of Fig. 13. Due to the decrease in signal intensity from $t_0 + 130$ ns, the ICCD gain was increased to visualize the weak emission up to approximately $5\,\mu$s. Here, the metal rod was the cathode and the glass surface was the anode (M^-D^+). First, the volume discharge touched the dielectric surface and a surface discharge developed along the embedded grid (t_0 and $t_0 + 10$ ns). This was followed by the development of a branching surface discharge that spread in a star-like shape along the embedded grid and inside this pattern along the surface ($t_0 + 40$ ns to $t_0 + 130$ ns). Then, a faint discharge in the volume and on both surfaces became visible ($t_0 + 430$ ns and $t_0 + 930$ ns) and even after about $5\,\mu$s an emission similar to that at t_0 occurred.
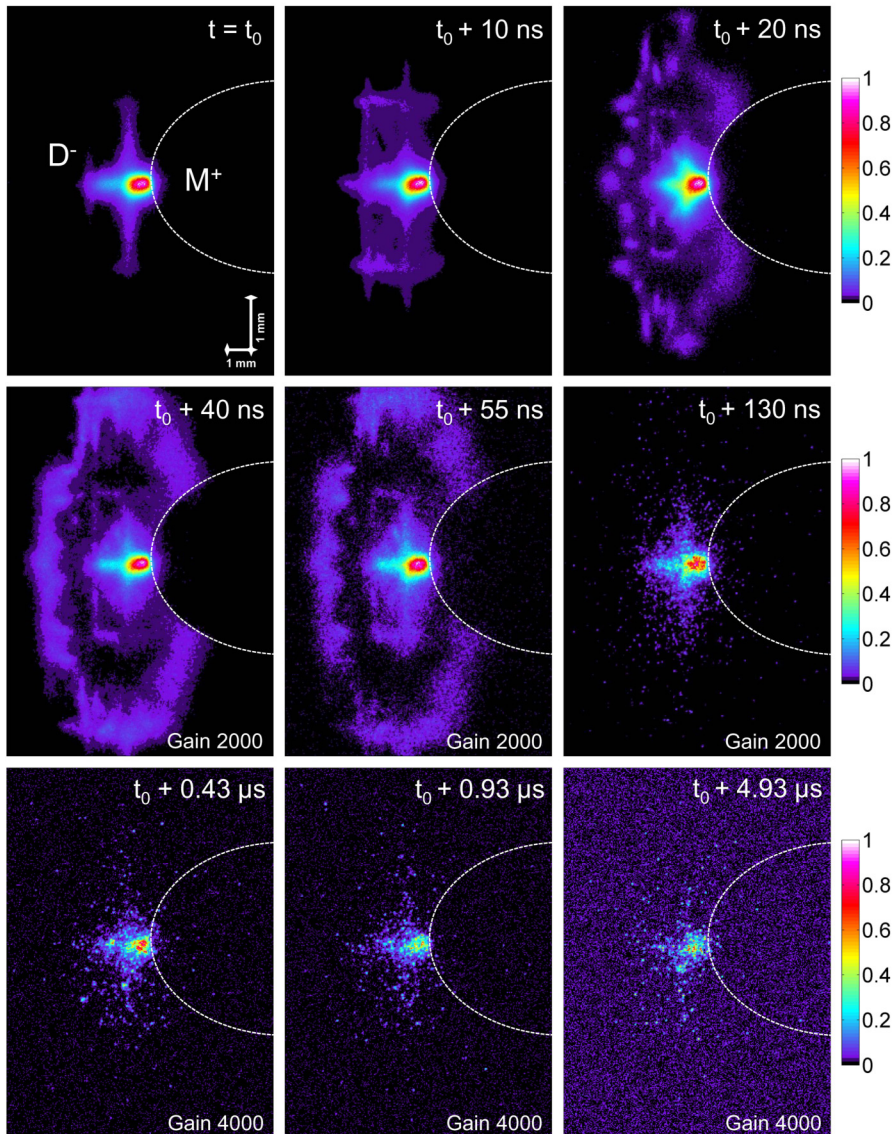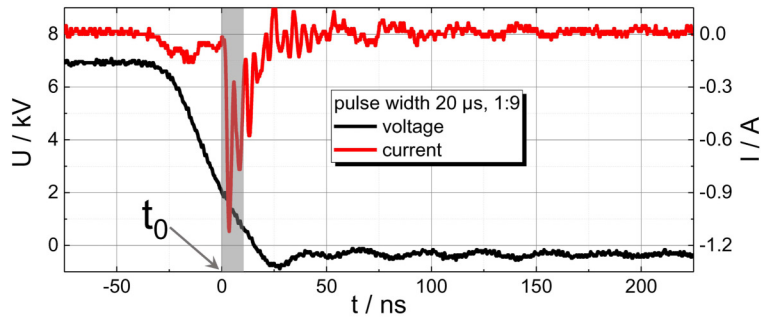
Figure 14 displays the temporal development of the surface discharge for +8 kV and a duty cycle of 1:9 during the falling slope (M^+D^-) using a 10 ns ICCD gate window. A duty cycle of 1:9 was chosen for the falling slope to compare with (M^-D^+) with the same delay to the preceding discharge and, therefore, a similar pre-ionization in the volume. The starting gate position was t_0. Again, due to the decrease in signal intensity from $t_0 + 40$ ns the ICCD gain was increased to visualize the weak emission up to approximately $5\,\mu$s. Here, the metal rod was the anode and the glass surface was the cathode (M^+D^-). Generally, the discharge emission was not as bright as for M^- and D^+. In the first phase, the volume discharge touched the dielectric surface and a surface discharge developed along the embedded grid (t_0 and $t_0 + 10$ ns) with emission at the nodes. In a second phase, a diffuse discharge developed from there and spread in a ring-like structure along the surface ($t_0 + 20$ ns to $t_0 + 60$ ns). Then, a faint discharge in the volume and on the dielectric surface close to the starting point became visible ($t_0 + 130$ ns to $t_0 + 1\,\mu$s), and even after about $5\,\mu$s, emission occurred in the volume close to the rod.

The grounded electrode was not covered by the dielectric, but it had a large radius of curvature, thereby avoiding electric field enhancement on the uncovered electrode. The charged electrode was covered by very thin (100 μm) glass, to ensure the lowest possible "blurring out" of the E-field lines by the dielectric. In addition, the glass-covered charged electrode, which was a mesh made of thin wires, therefore, a source of high E-field strength. Electrostatic

calculations in a similar setup but with a more extended metallic electrode[18] revealed that indeed a high electric field was present on the side of the glass-covered charged mesh, and not at the grounded electrode. The discharge, therefore, could easily be initiated both on the bare electrode and in the high E-field strength region on the pre-charged thin glass. As discussed in Ref. 18, this behavior is what caused the discharge to maintain its meshed structure throughout the volume discharge, even when a larger grounded electrode was used. In the current experiment, a small diameter electrode was used. If a similar electrode would have been placed underneath the thin dielectric, a concentrated discharge footprint could be observed; while an extended electrode underneath would result in the so-called Lichtenberg figures.[41] The electric field caused by the mesh structure that is covered by the thin dielectric maintains the surface discharge along the grid structure and its spreading.

For both polarities of the glass-covered mesh (D^+ and D^-), outstretched surface discharges on the glass occurred, following the geometry of the embedded mesh with diverse morphology. It is evident that a DBD with a thin dielectric layer covering a fine mesh electrode is an appropriate arrangement to establish widely spread almost homogeneous surface discharges guided by the mesh.

IV. CONCLUSIONS

Surface and volume discharges in a pulsed asymmetric dielectric barrier discharge between a glass covered mesh electrode and a grounded metal electrode in the atmospheric pressure air were measured and analyzed.

For discharge characteristics, the relationship between the polarities of the two electrodes was shown to be much more important than the polarity of the voltage pulse applied to the charged mesh. Both the current–voltage profiles and the imaging displayed remarkable similarities between the discharge developing during the rising slope of the positive pulse and during the falling slope of the negative pulse (M^-D^+). Similarly, the discharge behavior of the falling slope of the positive pulse much resembled that of the rising slope of the negative pulse (M^+D^-).

During the rising slope of the positive pulse (M^-D^+), the discharge was initiated in the volume and streamers developed toward both electrodes and continued propagating on the glass. The volume discharge was weaker, while an outstretched star-like surface discharge developed on the glass electrode sustained by the embedded mesh.

During the falling slope of the positive pulse (M^+D^-), a streamer was initiated in the volume close to the grounded electrode, propagating onto the glass-covered mesh and initiating a surface discharge there. The volume discharge featured a stronger emission, lasted longer, and the streamer velocity was higher (9:1).

It can be concluded that during the rising slope, the highest E-field strength and the highest energy electrons occurred at the grounded electrode, while the discharge on the surface was driven by lower-energy electrons in a lower E-field, thus exhibiting thinner filaments and following the underlying mesh. During the falling slope, the highest E-field region was on the mesh, resulting in a more diffuse surface discharge that did not always follow the underlying mesh structure.

Finally, the impact of the duty cycle (pulse width) on the discharge development and its properties was exerted through the effects of the gas phase and surface pre-ionization. A short delay after the preceding discharge resulted in less spatial and temporal uncertainties, as shown for positive HV pulses for the falling slope of a duty cycle of 1:9 and the rising slope of 9:1.

To conclude, the main benefit of the asymmetric DBD arrangement investigated here is the generation of widespread surface discharges using the filamentary regime, which is much stronger in the transferred charge and energy than diffuse DBDs.

ACKNOWLEDGMENTS

DATA AVAILABILITY

The data that support the findings of this study are available from the corresponding author upon reasonable request.

REFERENCES

[1]H. Boettner, J. Waskoenig, D. O'Connell, T. L. Kim, P. A. Tchertchian, J. Winter, and V. Schulz-von der Gathen, "Excitation dynamics of microstructured atmospheric pressure plasma arrays," J. Phys. D Appl. Phys. **43**, 124010 (2010).

[2]L. Zhao, W. Liu, Z. Li, and C. Ma, "Study of surface atmospheric pressure glow discharge plasma based on ultrathin laminated electrodes in air," Phys. Plasmas **25**, 053515 (2018).

[3]R. Tschiersch, S. Nemschokmichal, M. Bogaczyk, and J. Meichsner, "Self-stabilized discharge filament in plane-parallel barrier discharge configuration: Formation, breakdown mechanism, and memory effects," J. Phys. D Appl. Phys. **50**, 415206 (2017).

[4]G. Fridman, G. Fridman, A. Gutsol, A. B. Shekhter, V. N. Vasilets, and A. Fridman, "Applied plasma medicine," Plasma Process. Polym. **5**, 503–533 (2008).

[5]M. G. Kong, G. Kroesen, G. Morfill, T. Nosenko, T. Shimizu, J. van Dijk, and J. L. Zimmermann, "Plasma medicine: An introductory review," New J. Phys. **11**, 115012 (2009).

[6]K.-D. Weltmann, E. Kindel, T. von Woedtke, M. Hähnel, M. Stieber, and R. Brandenburg, "Atmospheric-pressure plasma sources: Prospective tools for plasma medicine," Pure Appl. Chem. **82**, 1223–1237 (2010).

[7]J. Hirschberg, T. Omairi, N. Mertens, A. Helmke, S. Emmert, and W. Viöl, "Influence of excitation pulse duration of dielectric barrier discharges on biomedical applications," J. Phys. D Appl. Phys. **46**, 165201 (2013).

[8]T. von Woedtke, S. Reuter, K. Masur, and K.-D. Weltmann, "Plasma for medicine," Phys. Rep. **51**, 291–320 (2013).

[9]R. Tiede, J. Hirschberg, W. Viöl, and S. Emmert, "A s-pulsed dielectric barrier discharge source: Physical characterization and biological effects on human skin fibroblasts," Plasma Processes Polym. **13**, 775–787 (2016).

[10]M. Laroussi, X. Lu, and M. Keidar, "Perspective: The physics, diagnostics, and applications of atmospheric pressure low temperature plasma sources used in plasma medicine," J. Appl. Phys. **122**, 020901 (2017).

[11]S. Reuter, T. von Woedtke, and K.-D. Weltmann, "The kINPen—A review on physics and chemistry of the atmospheric pressure plasma jet and its applications," J. Phys. D Appl. Phys. **51**, 233001 (2018).

[12]B. Boekema, M. Vlig, D. Guijt, K. Hijnen, S. Hofmann, P. Smits, A. Sobota, E. M. van Veldhuizen, P. Bruggeman, and E. Middelkoop, "A new flexible DBD device for treating infected wounds: In vitro and ex vivo evaluation and comparison with a RF argon plasma jet," J. Phys. D Appl. Phys. **530**, 044001 (2016).

[13]S. Okazaki, M. Kogoma, M. Uehara, and Y. Kimura, "Appearance of stable glow discharge in air, argon, oxygen and nitrogen at atmospheric pressure using a 50 Hz source," J. Phys. D Appl. Phys. **26**, 889–892 (1993).

[14]X. Wang, H. Luo, Z. Liang, T. Mao, and R. Ma, "Influence of wire mesh electrodes on dielectric barrier discharge," Plasma Sources Sci. Technol. **15**, 845–848 (2006).

[15]Z. Fang, Y. Qiu, C. Zhang, and E. Kuffel, "Factors influencing the existence of the homogeneous dielectric barrier discharge in air at atmospheric pressure," J. Phys. D Appl. Phys. **40**, 1401–1407 (2007).

[16]M. C. Paliwoda and J. L. Rovey, "Intensity control of individual DBD plasma filament. I. Experiment with a needle electrode," Phys. Plasmas **24**, 053504 (2017).

[17]Q. Ye, Y. Wu, X. Li, T. Chen, and G. Shao, "Uniformity of dielectric barrier discharges using mesh electrodes," Plasma Sources Sci. Technol. **21**, 065008 (2012).

[18]M. van der Schans, A. Sobota, and G. M. W. Kroesen, "Dielectric barrier discharge in air with a controllable spatial distribution—A tomographic investigation," J. Phys. D Appl. Phys. **49**, 195204 (2016).

[19]T. Hoder, R. Brandenburg, R. Basner, K.-D. Weltmann, K. V. Kozlov, and H.-E. Wagner, "A comparative study of three different types of barrier discharges in air at atmospheric pressure by cross-correlation spectroscopy," J. Phys. D Appl. Phys. **43**, 124009 (2010).

[20]Y. Akishev, G. Aponin, A. Balakirev, M. Grushin, V. Karalnik, A. Petryakov, and N. Trushkin, "'memory' and sustention of microdischarges in a steady-state DBD: Volume plasma or surface charge?," Plasma Sources Sci. Technol. **20**, 024005 (2011).

[21]S.-W. Xu, F. He, Y. Wang, L. Li, and J.-T. Ouyang, "Effect of volume and surface charges on discharge structure of glow dielectric barrier discharge," Phys. Plasmas **20**, 083515 (2013).

[22]S. Nemschokmichal, R. Tschiersch, H. Höft, R. Wild, M. Bogaczyk, M. M. Becker, D. Loffhagen, L. Stollenwerk, M. Kettlitz, R. Brandenburg, and J. Meichsner, "Impact of volume and surface processes on the pre-ionization of dielectric barrier discharges: Advanced diagnostics and fluid modeling," Eur. Phys. J. D **72**, 89 (2018).

[23]P. Bruggeman and R. Brandenburg, "Atmospheric pressure discharge filaments and microplasmas: Physics, chemistry and diagnostics," J. Phys. D Appl. Phys. **46**, 464001 (2013).

[24]G. B. Sretenovic, I. B. Krstic, V. V. Kovacevic, B. M. Obradovic, and M. M. Kuraica, "Spatio-temporally resolved electric field measurements in helium plasma jet," J. Phys. D Appl. Phys. **47**, 102001 (2014).

[25]B. M. Goldberg, I. Shkurenkov, S. O'Byrne, I. V. Adamovich, and W. R. Lempert, "Electric field measurements in a dielectric barrier nanosecond pulse discharge with sub-nanosecond time resolution," Plasma Sources Sci. Technol. **24**, 035010 (2015).

[26]P. Böhm, M. Kettlitz, R. Brandenburg, H. Höft, and U. Czarnetzki, "Determination of the electric field strength of filamentary DBDs by cars-based four-wave mixing," Plasma Sources Sci. Technol. **25**, 054002 (2016).

[27]R. Ono, "Optical diagnostics of reactive species in atmospheric-pressure nonthermal plasma," J. Phys. D Appl. Phys. **49**, 083001 (2016).

[28]Y. Inada, A. Komuro, R. Ono, A. Kumada, K. Hidaka, and M. Maeyama, "Two-dimensional electron density measurement of pulsed positive secondary streamer discharge in atmospheric-pressure air," J. Phys. D Appl. Phys. **52**, 185204 (2019).

[29]M. Hofmans and A. Sobota, "Influence of a target on the electric field profile in a kHz atmospheric pressure plasma jet with the full calculation of the Stark shifts," J. Appl. Phys. **125**, 043303 (2019).

[30]K. Tomita, Y. Inada, A. Komuro, X. Zhang, K. Uchino, and R. Ono, "Measurement of electron velocity distribution function in a pulsed positive streamer discharge in atmospheric-pressure air," J. Phys. D Appl. Phys. **53**, 08LT01 (2020).

[31]A. Komuro, K. Suzuki, K. Yoshida, and A. Ando, "Characteristics of spatio-temporal variations of primary and secondary streamers under pulsed-voltage in air at atmospheric pressure," Jap. J. Appl. Phys. **59**, SAAB03 (2020).

[32]M. Kettlitz, H. Höft, T. Hoder, S. Reuter, K.-D. Weltmann, and R. Brandenburg, "On the spatio-temporal development of pulsed barrier discharges: Influence of duty cycle variation," J. Phys. D. Appl. Phys. **45**, 245201 (2012).

[33]K. V. Kozlov, R. Brandenburg, H.-E. Wagner, A. M. Morozov, and P. Michel, "Investigation of the filamentary and diffuse mode of barrier discharges in N_2/O_2 mixtures at atmospheric pressure by cross-correlation spectroscopy," J. Phys. D Appl. Phys. **38**, 518–529 (2005).

[34]S. Jahanbakhsh, V. Brüser, and R. Brandenburg, "Single microdischarges in a barrier corona arrangement with an anodic metal pin: Discharge characteristics in subsequent breakdowns," Plasma Sources Sci. Technol. **27**, 115011 (2018).

[35]K. V. Kozlov, H.-E. Wagner, R. Brandenburg, and P. Michel, "Spatio-temporally resolved spectroscopic diagnostics of the barrier discharge in air at atmospheric pressure," J. Phys. D Appl. Phys. **34**, 3164–3176 (2001).

[36]A. Lofthus and P. H. Krupenie, "The spectrum of molecular nitrogen," J. Phys. Chem. **6**, 113 (1977).

[37]T. Hoder, H. Höft, M. Kettlitz, K.-D. Weltmann, and R. Brandenburg, "Barrier discharges driven by sub-microsecond pulses at atmospheric pressure: Breakdown manipulation by pulse width," Phys. Plasmas **19**, 070701 (2012).

[38]H. Höft, M. Kettlitz, M. M. Becker, T. Hoder, D. Loffhagen, R. Brandenburg, and K.-D. Weltmann, "Breakdown characteristics in pulsed-driven dielectric barrier discharges: Influence of the pre-breakdown phase due to volume memory effects," J. Phys. D Appl. Phys. **47**, 465206 (2014).

[39]M. Kettlitz, H. Höft, T. Hoder, K.-D. Weltmann, and R. Brandenburg, "Comparison of sinusoidal and pulsed-operated dielectric barrier discharges in an O_2/N_2 mixture at atmospheric pressure," Plasma Sources Sci. Technol. **22**, 025003 (2013).

[40]D. Braun, V. Gibalov, and G. Pietsch, "Two-dimensional modelling of the dielectric barrier discharge in air," Plasma Sources Sci. Technol. **1**, 166–174 (1992).

[41]V. I. Gibalov and G. J. Pietsch, "Dynamics of dielectric barrier discharges in different arrangements," Plasma Sources Sci. Technol. **21**, 024010 (2012).